Talanta 200 (2019) 293–299

Contents lists available at ScienceDirect

Talanta

journal homepage: www.elsevier.com/locate/talanta

Adsorption of cholesterol oxidase and entrapment of horseradish peroxidase in metal-organic frameworks for the colorimetric biosensing of cholesterol

Mengyuan Zhao[a,b], Yao Li[a,b], Xuejuan Ma[a,b], Mengfan Xia[a,b], Yaodong Zhang[a,b,*]

[a] Key Laboratory of Analytical Chemistry for Life Science of Shaanxi Province, School of Chemistry and Chemical Engineering, Shaanxi Normal University, Changan West Road 620, 710119 Xi'an, China

[b] Key Laboratory of Applied Surface and Colloid Chemistry of Ministry of Education, School of Chemistry and Chemical Engineering, Shaanxi Normal University, Changan West Road 620, 710119 Xi'an, China

ARTICLE INFO

Keywords:
Co-immobilization
Cholesterol oxidase
Horseradish peroxidase
Metal–organic frameworks
Colorimetric
Cholesterol

ABSTRACT

The co-immobilization of two enzymes onto single support commonly exhibits low efficiency due to the competition against limited sites. Water-stable metal–organic frameworks (MOFs) [i.e., PCN-333(Al)] with a high surface area and ultra-large cavities were employed to efficiently adsorb cholesterol oxidase (ChOx) and encapsulate horseradish peroxidase (HRP), respectively. The prepared PCN-333/ChOx&HRP was characterized through SEM, XRD, confocal microscopy, N_2 adsorption isotherms, and thermal gravity analysis (TGA). The high surface area and high concentration of mesoporous cages resulted in the high loadings of both ChOx and HRP. The absorbed ChOx and the encapsulated HRP presented excellent activities without additional chemical modification. The immobilized enzymes were stable against protease digestion, organic solvents, temperature changes, and pH variation. Thus, a colorimetric biosensor for cholesterol detection was fabricated depending on cascade catalytic reactions of the immobilized bi-enzymes. An extended linear range from 0.0 to 40.0 μM with a low detection limit of 0.6 μM was obtained using the biosensor. The co-immobilization of the enzymes onto the surface and into the mesopores of MOFs provided a new and excellent platform for the development of highly stable and sensitive colorimetric biosensors.

1. Introduction

Various multi-enzymatic systems have been developed to catalyze cascade reactions [1]. For instance, eight enzymes are involved in the citric acid cycle to effectively metabolize sugars, fats, and proteins. Inspired by nature, researchers coupled multiple enzymes for synthesis and industrial production in a cascade manner [2]. Enzyme immobilization offers the benefit of stability, recovery, and reuse of expensive biocatalysts. Thus far, the strategy for enzyme immobilization can be classified into four main categories, namely, surface attachment (adsorption), covalent cross-linking, pore encapsulation, and co-precipitation [3]. Immobilizing enzymes, which are not involved in chemical modification, can finely retain the performance of free enzymes and show superior stability because of the fragile nature of enzymes [4]. Different kinds of porous materials, such as mesoporous silica, sol–gel matrices, and phospholipid liposomes, have been utilized to construct various enzymatic cascade reaction [5,6]. However, challenges related to rational structural designs, entry of bulky substrates, and leaching of enzymes from support hinder the use of such supports.

Metal–organic frameworks (MOFs) are attractive candidates for enzyme immobilization because of their chemical and thermal stability, high surface area, tunable porosity, and mild synthetic conditions [3,7–10]. Various MOFs have been applied to immobilize different enzymes, such as organophosphorus acid anhydrolase [11], glycerol dehydrogenase [12], glucose dehydrogenase [13], pectinase [14] , lipase [15], trypsin [16], and urease [17–21]. Encapsulated enzymes in MOFs exhibit excellent recyclability and stability. Pisklak and coworkers [22] reported for the first time an approach that involves the adsorption of microperoxidase-11 into the cavity of Cu-MOF. Zhou et al. [23] demonstrated a series of stable MOFs with ultra-large pores as single-molecule traps for enzyme encapsulation. Highly stable MOFs [PCN-333(Al)] have a pore diameter of 5.5 nm × 4.2 nm and a large pore volume and are suitable for enzyme encapsulation.

* Corresponding author at: Key Laboratory of Analytical Chemistry for Life Science of Shaanxi Province, School of Chemistry and Chemical Engineering, Shaanxi Normal University, Changan West Road 620, 710119 Xi'an, China.
E-mail address: ydzhang@snnu.edu.cn (Y. Zhang).

https://doi.org/10.1016/j.talanta.2019.03.060
Received 21 December 2018; Received in revised form 28 February 2019; Accepted 14 March 2019
Available online 15 March 2019

Cholesterol maintains the structural integrity and fluidity of animal cell membranes and acts as a precursor for the biosynthesis of steroid hormones, bile acids, and vitamin D. In healthy human serum, the desirable concentration of cholesterol is 200 mg/dL. Unregulated cholesterol levels in the human body can lead to serious diseases, such as hypertension, cardiac arrest, coronary heart and peripheral arterial diseases, diabetes, and anemia [24]. Many methods are used to detect cholesterol, such as fluorometry [25,26], electrochemical methods [27–33], molecular imprinting technology [34], chromatography [35,36], and colorimetric enzymatic assays [37]. However, some detection methods require expensive equipment [26,36,38] or have low sensitivity [30,34]. Therefore, a convenient and cost-efficient sensor suitable for point-of-care diagnostics should be developed.

Such a colorimetric strategy is feasible on a point-of-care platform [39]. Cholesterol oxidase (ChOx) and horseradish peroxidase (HRP) mediate a two-step colorimetric reaction for cholesterol detection. ChOx oxidizes cholesterol to produce H_2O_2, and HRP catalyzes the chromogenic oxidation reaction of substrates with H_2O_2. This bi-enzyme cascade reaction is highly specific and efficient; however, the decomposition of H_2O_2 largely reduces the accuracy and sensitivity of assays [40]. Moreover, the overall cost of assays must be considered when expensive enzymes are utilized [41]. As such, strategies for the immobilization of ChOx and HRP have been exploited [42]. However, the efficiency of the co-immobilization of bi-enzymes commonly decreases because of site limitations.

Herein, ChOx was first absorbed onto the surface of PCN-333(Al), and HRP was successively diffused into the large pores of PCN-333(Al) because of the high surface area, large pore diameter (5.5 nm) of PCN-333(Al), and the sizes of ChOx (size: 5.13 nm × 6.30 nm × 7.30 nm) and HRP (size: 4.0 nm × 4.4 nm × 6.8 nm). Thus, ChOx and HRP were efficiently co-immobilized and had an excellent cascade catalytic performance. MOFs immobilized with the two enzymes could be used as a tandem sensor for the colorimetric detection of cholesterol (Scheme 1).

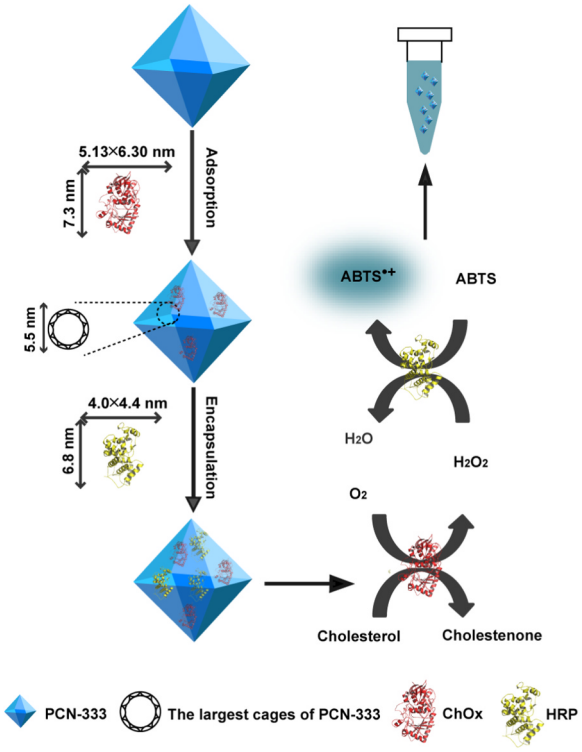

Scheme 1. Schematic of the co-immobilization of ChOx and HRP and for cholesterol detection.

2. Experimental section

2.1. Materials and instruments

ChOx (> 10 U/mg) from microorganisms and *N,N′*-diethylformamide (DEF) were purchased from Aladdin Chemistry Company. (Shanghai, China). HRP (≥300 U/mg), cholesterol, 2,2′-azinobis-(3-ethylbenzothiazoline-6-sulphonate) (ABTS), and rhodamine B (RhB) were obtained from Sangon Biotechnology (Shanghai, China). 4,4′,4′-s-Triazine-2,4,6-triyl-tribenzoic acid (H_3TATB, 95%) and fluorescein isothiocyanate (FITC) were procured from Sigma-Aldrich (Shanghai, China). The human serums were donated by an affiliated hospital of Shaanxi Normal University. All other chemicals used in this work were of analytical grade and used without further purification.

UV-vis spectra were obtained using a Lambd-35 spectrophotometer (Perkin Elmer, America) . SEM images were recorded with a SU8220 scanning electron microscope (Hitachi, Japan). The powder X-ray diffraction (XRD) patterns of the as-prepared products were performed on a D8 Advance X-ray diffractometer (Bruker, Germany). Nitrogen adsorption–desorption isotherms were obtained with an ASAP2460 surface area and porosity analyzer at 77 K (Micromeritics, America) . Thermal gravimetric analysis (TGA) was conducted on a Q600SDT thermoanalyzer systems under nitrogen atmosphere (25–800 °C) at a heating rate of 10 °C min^{-1} (TA, America) . Confocal fluorescence images were carried out on a FV1200 confocal laser scanning microscope under ambient conditions (Olympus, Japan) .

2.2. Preparation of PCN-333

A mixture of H_3TATB (50 mg) and $AlCl_3{\cdot}6H_2O$ (200 mg) was dissolved in DEF (10 mL) through ultrasonication for 30 min, and 1.0 mL of trifluoroacetic acid was added to the obtained mixture. After 10 min of ultrasonication, the mixture was heated in an oven at 135 °C for 2 days until a white precipitate formed. The white precipitate was centrifuged and washed with fresh DEF several times. Finally, the product was dried under vacuum at 45 °C for 3 days.

2.3. Preparation of PCN-333/ChOx&HRP

PCN-333/ChOx&HRP was prepared as follows: 6 mg of as-synthesized PCN-333 was dispersed in 500 μL of deionized water, and 500 μL of 2 mg/mL ChOx solution was added to the MOF slurry and stirred at 37 °C for 40 min. The solid was collected through centrifugation and washed with DI water twice. MOF was re-dispersed in 500 μL of water. Afterward, 500 μL of 1 mg/mL HRP solution was added to the MOF slurry and stirred at 37 °C for another 40 min. The solid was collected through centrifugation, washed with water twice, diluted in 1000 μL of phosphatic buffer solution (0.02 M, pH 7.5), and finally stored at 4 °C in a refrigerator.

The supernatants were collected for the determination of the amount of immobilized enzymes in PCN-333.

2.4. Preparation of the PCN-333/RhB-ChOx and FITC-HRP

For the synthesis of RhB-ChOx, ChOx (1 mg) and RhB (2 mg) were dissolved in 500 μL of phosphatic buffer solution (0.02 M, pH 7.5). The solution was stirred at 4 °C for 24 h. The mixture was dialyzed against distilled water for 24 h by using a membrane with a molecular weight cut-off of 8000–14,000 Da. FITC-HRP was synthesized using a similar procedure.

For the preparation of PCN-333/RhB-ChOx and FITC-HRP, 6 mg of the as-synthesized PCN-333 was dispersed in 500 μL of deionized water, and 500 μL of RhB-ChOx was added to the MOF slurry and shaken at 37 °C for 40 min. The solid was collected through centrifugation and washed with DI water twice. MOF was re-dispersed in 500 μL of water, and 500 μL of FITC-HRP solution was added to the MOF slurry and

shaken at room temperature for another 40 min. The solid was obtained through centrifugation, washed with water twice, diluted in 1000 μL of phosphatic buffer solution (0.02 M, pH 7.5), and observed through confocal laser scanning microscopy (CLSM).

2.5. Colorimetric detection of cholesterol with PCN-333/ChOx&HRP

The cascade enzymatic activity of PCN-333/ChOx&HRP was evaluated on the basis of the oxidation of cholesterol and chromogenic substrate ABTS. A stock solution of cholesterol was used, and the mixture of isopropanol and Triton X-100 (1:1) was used to dissolve cholesterol. The standard cholesterol solutions were diluted with phosphatic buffer solution (0.02 M, pH 7.5) and stored at 4 °C. For cholesterol determination, 10 μL of 0.0–40.0 μM cholesterol was added to 90 μL of phosphatic buffer solution (0.02 M, pH 7.5), and 10 μL of the as-prepared PCN-333/ChOx&HRP was incubated at 37 °C in the dark for 30 min. Afterward, 840 μL of acetate buffer (0.02 M, pH 4.0) and 50 μL of 10 μmol/mL ABTS solution were added to the obtained mixture. The mixture was incubated at 37 °C in the dark for 10 min. The reaction solution was centrifuged at 145,000 rpm for 3 min to remove PCN-333/ChOx&HRP particles. The supernatant was measured using a UV spectrophotometer, and the maximum absorbance of $ABTS^{\bullet+}$ was recorded at 418 nm.

2.6. Detection of cholesterol in serum

For the determination of free cholesterol in serum, a standard addition method was used to detect cholesterol. The serum was pretreated before detection to prevent the influence of other matrices. In particular, 0.2 mL of human serum sample was diluted with the mixture of 1.8 mL of ethanol solution and 2.0 mL of water. Then, the diluted samples were added with 4.0 mL of n-hexane and centrifuged for 5 min. The section of n-hexane extract was allowed to stand for a few minutes and separated. The solvent was then evaporated into residue. Finally, the residue was re-dissolved with the mixture of isopropanol and Triton X-100 (1:1).

To take the above 50 μL serum into 50 μL phosphatic buffer solution (0.02 M, pH 7.5), and 10 μL of PCN-333&ChOx/HRP was added to the aforementioned mixture and incubated at 37 °C in the dark for 30 min. Afterward, 840 μL of acetate buffer (0.02 M, pH 4.0) and 50 μL of 10 μmol/mL ABTS were added. The mixture was incubated at 37 °C in the dark for 10 min. Finally, the mixture was centrifuged at 14,500 rpm for 3 min to remove PCN-333/ChOx&HRP. The supernatant was examined using a UV spectrophotometer, and the maximum absorbance of $ABTS^{\bullet+}$ was recorded at 418 nm.

3. Results and discussion

3.1. Characterization of PCN-333/ChOx&HRP

Because PCN-333 (Al) has high void volumes (3.84 $cm^3\ g^{-1}$) and three cage types (diameter :5.5, 3.4, and 1.1 nm), it is an ideal candidate for enzyme loading [23]. The overall procedure for the co-immobilized ChOx and HRP onto/into PCN-333 and the detection mechanism of cholesterol are illustrated in Scheme 1. PCN-333 was synthesized as described in literature [23]. To characterize the morphological characteristics of PCN-333, we performed scanning electron microscopy (SEM) (Fig. 1A). MOFs were uniformly dispersed in the solution and showed an octahedron morphology with an average size of around 2 μm. Considering the sizes of ChOx (5.13 nm × 6.30 nm × 7.30 nm) and HRP (4.0 nm × 4.4 nm × 6.8 nm), we first immobilized ChOx through surface absorption, and HRP was encapsulated through diffusion. In this case, the calculated loadings were 0.06 g g^{-1} for ChOx and 0.08 g g^{-1} for HRP. PCN-333/ChOx&HRP also displayed the same morphology as that of PCN-333 (Fig. 1B). The retained bulk crystallinity and morphology of PCN-333 indicated that the immobilized enzyme molecules did not alter the morphology of MOFs.

The crystal structures of the related PCN-333 products were tested through powder XRD. The positions and corresponding intensities of all the diffraction peaks matched well by comparing those from the as-synthesized PCN-333 and PCN-333/ChOx&HRP with that from simulated PCN-333(Fig. 1C). Therefore, enzyme immobilization did not disturb the crystal construction of PCN-333 and still maintained good crystalline integrity after immobilization was completed.

TGA was employed to quantitatively determine the composition of PCN-333/ChOx&HRP (Fig. 1D). The first decomposition stage of both PCN-333 and the composite exhibited a gradual weight loss of ~10% up to ca.100 °C corresponding to the removal of some unreacted reagents and the guest molecules from the cavities. The second-stage decomposition of the composite started from 250 °C and finished at around 500 °C, whereas PCN-333 had much less weight loss during this stage. About 11 wt% of weight loss of the composite were found at the second stage possibly because of the decomposition of protein molecules, and this finding was consistent with the results of the enzyme loading calculations. The weight loss in PCN-333 and PCN-333/ChOx&HRP over 500 °C was associated with the thermal decomposition of PCN-333 crystals.

To test the extent of pore filling, the porous features of PCN-333 before and after enzyme immobilization were also investigated with nitrogen sorption isotherms. The N_2 uptake capacity of PCN-333/ChOx&HRP was lower than that of PCN-333. Two steep increases at $P/P_0 = 0.30$ and 0.45 on the N_2 adsorption isotherm corresponded to two types of mesoporous cages in PCN-333. Brunauer–Emmett–Teller (BET) surface area decreased from 2550 m^2/g to 603 m^2/g after saturation with ChOx and HRP occurred (Fig. 1E), indicating that a majority of the free space in PCN-333 was occupied by enzyme molecules. Pore size distribution analysis in based on density functional theory (DFT) revealed that the pore size of PCN-333/ChOx&HRP was around 3–5 nm (Fig. 1F). Furthermore, the pore volume decreased from 2.48 cm^3/g to 0.43 cm^3/g after ChOx and HRP immobilization (Fig. 1F). The pore-size distribution diagrams of individual HRP and ChOx immobilized with PCN-333 are different (see Supplementary information, Figs. S1-S4), indicated that HRP and ChOx were immobilized in different way. Notably, the distribution of the largest cavity has obviously decreased in PCN-333/HRP, but not in PCN-333/ChOx, which signify the entrapment of HRP and adsorption of ChOx [43].

Confocal laser scanning microscopy (CLSM) was conducted to confirm whether ChOx and HRP were immobilized in PCN-333. ChOx and HRP were labeled with RhB and FITC, respectively, and the two labeled-enzymes were immobilized in the same synthesis procedure. The fluorescence signal originated from RhB-ChOx and FITC-HRP because the PCN-333 material itself was not a fluorescence material (Fig. 2). The experimental results indicated the presence and random distribution of ChOx and HRP in the overall framework structure of PCN-333.

To investigate and compare the catalytic activity of PCN-333/ChOx&HRP in a cascade reaction, we prepared PCN-333/ChOx and PCN-333/HRP systems. The prepared PCN-333/ChOx and PCN-333/HRP were immobilized with the same amount of enzymes as that of PCN-333/ChOx&HRP. ChOx catalyzes the reaction between molecular oxygen. The generated hydrogen peroxide was reduced in the conversion of ABTS to $ABTS^{\bullet+}$ as catalyzed by HRP and monitored at 418 nm through UV–vis spectroscopy. PCN-333 itself did not have any activity on cholesterol in the cascade reaction under the same reaction conditions (Fig. 3A). The activity of PCN-333/ChOx&HRP was 1.94 times higher than that of the mixture of PCN-333/ChOx and PCN-333/HRP (Fig. 3A). The results indicated that the catalytic rate of PCN-333/ChOx&HRP for cholesterol detection was faster than that of the mixture. The increase in the activity was due to the simultaneous encapsulation of ChOx and HRP in the same PCN-333 structure, and H_2O_2 produced by ChOx could react with ABTS immediately in the presence of HRP. However, intermediates needed to be released from the PCN-333/ChOx framework and enter the PCN-333/HRP framework to react. The

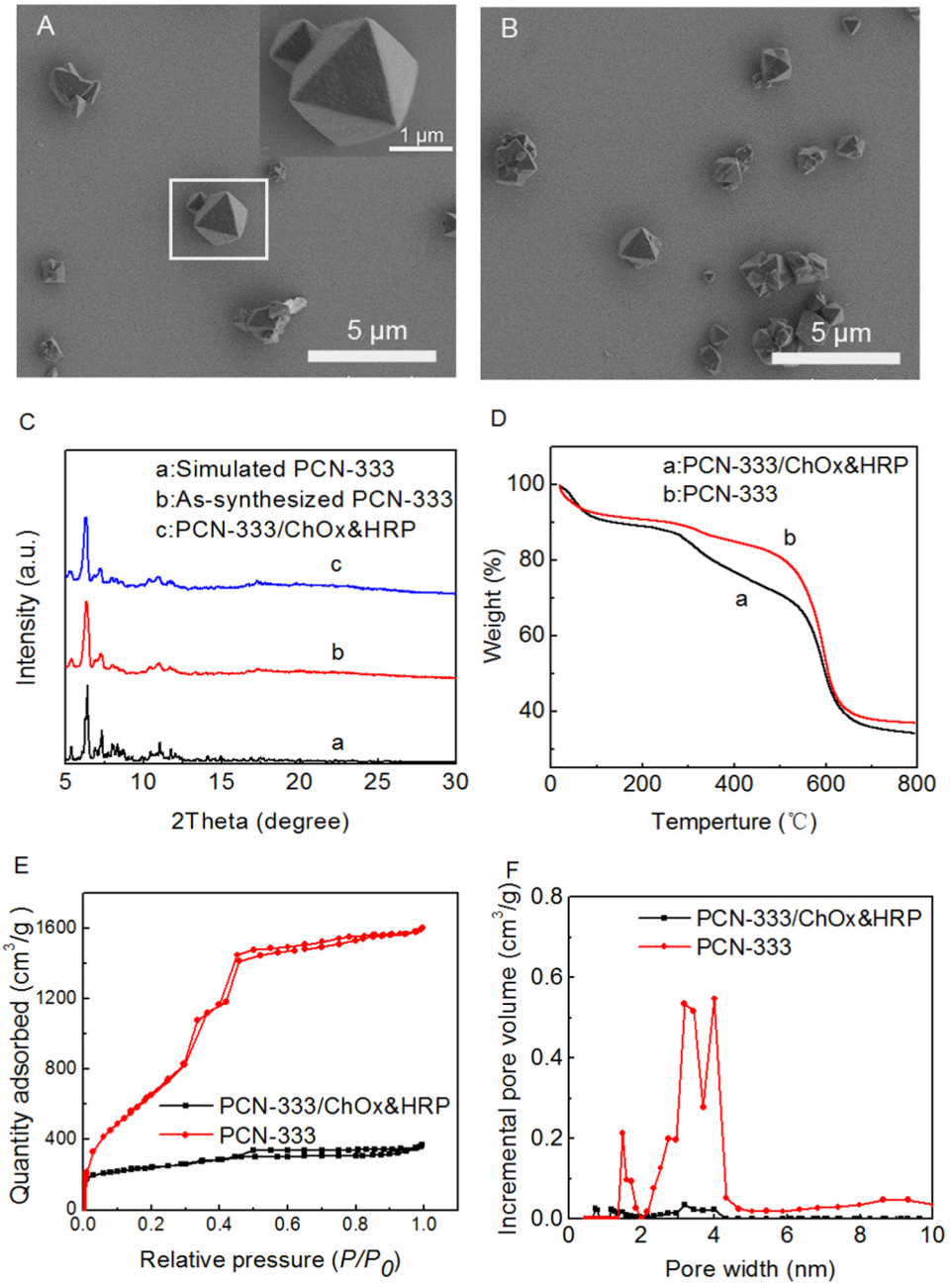

Fig. 1. SEM images of (A) PCN-333 and (B) PCN-333/ChOx&HRP composite. (C) XRD patterns of simulated PCN-333, as-synthesized PCN-333, and PCN-333/ChOx&HRP composite. (D) TGA curves of PCN-333 and PCN-333/ChOx&HRP composite. (E) N_2 sorption isotherms of PCN-333/ChOx&HRP composite and PCN-333. (F) Pore size distributions of PCN-333/ChOx&HRP composite and PCN-333.

increasing diffusion distance and decomposition of intermediates could significantly reduce the cascade reaction rate for PCN-333/ChOx and PCN-333/HRP systems. Considering that the number of empty cages (i.e., 3.4 and 1.1 nm) of PCN-333 greatly facilitated the diffusion of substrates and products, we observed an enhanced catalytic performance of PCN-333/ChOx&HRP.

3.2. Stability of PCN-333/ChOx&HRP

The stability of immobilized enzyme is essential for applications. To evaluate the stability of PCN-333/ChOx&HRP, we prepared the mixture of free enzymes with 0.2 μM ChOx and 0.2 μM HRP for comparison and tested the stability of co-immobilized ChOx and HRP against protease and organic solvents. PCN-333/ChOx&HRP incubated with trypsin for 30 min remained at 90%, and the activity of the mixed free enzyme was maintained at 29% of the initial activity (Fig. S5). PCN-333/ChOx&HRP incubated with isopropanol or 50% ethanol for 15 min was maintained at 71% or 61%. In comparison with the activity of the mixed free ChOx and HRP, the activity of PCN-333/ChOx&HRP did not significantly decrease in the presence of trypsin, isopropanol, or 50% ethanol (Fig. S5). This observation fully demonstrated that the channel of MOF formed a barrier when trypsin, isopropanol, and 50% ethanol were closed to enzyme molecules reducing the activity loss of ChOx and HRP.

To evaluate thermal stability, we assessed the activity of the mixed free enzymes and PCN-333/ChOx&HRP to the same concentration of cholesterol at different temperatures (25–75 °C). At 25–45 °C, the activity of two systems barely changed (Fig. S6). When the temperature was increased to 50 °C, the activity of the mixed free enzymes was

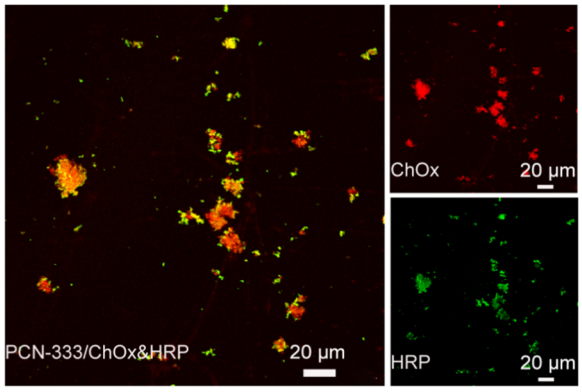

Fig. 2. Confocal laser scanning microscopy images of the PCN-333/ChOx&HRP (left column, merged picture). ChOx = red and HRP = green. (For interpretation of the references to color in this figure legend, the reader is referred to the web version of this article)

retained at 78%, and PCN-333/ChOx&HRP decreased by 4%. We further increased the incubation temperature to 55 °C, and the activity of the mixed free enzymes was 25% of their initial activity. On the contrary, PCN-333/ChOx&HRP remained at 88% of its initial activity. The low thermal stability of the mixed free enzymes might be caused by the partial inactivation of the free enzymes after the specimen was incubated at high temperatures. The stability under different acidic conditions is another crucial factor of immobilized enzymes. PCN-333/ChOx&HRP and the mixed free enzymes were incubated at different pH for 2 h, and the activity of PCN-333/ChOx&HRP was obviously higher than mixed free ChOx and HRP (Fig. S7). The protective effect of the highly stable PCN-333 rigid structure activated the enzymatic protein conformation of ChOx and HRP at different temperatures and pH to prevent enzyme deactivation.

The long-term storage stability of the co-immobilized enzymes were also essential for biotechnological applications. The mixed free enzymes and PCN-333/ChOx&HRP were incubated in phosphatic buffer solution (0.02 M, pH 7.5) at room temperature (Fig. S8), respectively. The relative activity of the free enzyme and the complex was compared at 0–20 days by taking a certain volume. PCN-333/ChOx&HRP retained 50% of the initial overall activity for 20 days. However, the relative activity of the mixed free enzymes was seriously lost and reduced by 84%, indicating that a large number of the mixed free enzymes were deactivated as time was extended. However, PCN-333 maintained a relatively high activity and long-term stability, indicating that PCN-333/ChOx&HRP could reduce the loss of enzyme activity due to its solid crystal structure. PCN-333/ChOx&HRP activity slightly changed in a refrigerator at 4 °C for 14 days (Fig. S9), and the MOF structure could improve the ability of the enzyme against a wide variety of external factors.

3.3. Assay performance of PCN-333/ChOx&HRP as colorimetric sensors

We detected cholesterol by using PCN-333/ChOx&HRP composite and by using ABTS as the chromogenic substrate in the enzyme cascade reaction. We investigated the activity of the bi-enzyme system by changing the mass ratio of ChOx and HRP from 2:1–6:1 (Figs. S10-S12) given that the influence of two enzymes mass ratios might play an important role in a cascade reaction. The least amounts of ChOx and HRP used for immobilization were observed at the 2:1 activity ratio. However, the obtained PCN-333/ChOx&HRP could achieve the ideal catalytic activity. Thus, the mass ratio of ChOx/HRP 2:1 was selected for the experimental study.

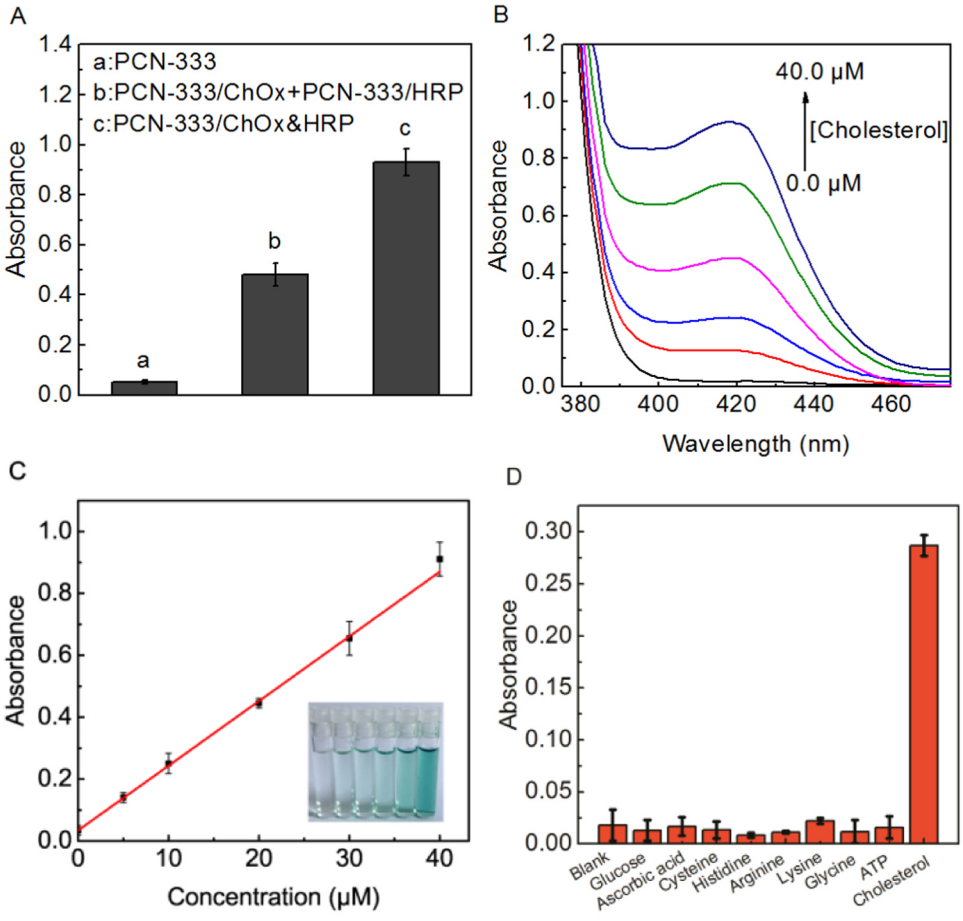

Fig. 3. (A) Comparison of the catalytic activity of PCN-333, PCN-333/ChOx, PCN-333/HRP, and PCN-333/ChOx&HRP. (B) UV–vis spectra of the mixed solutions of ABTS and PCN-333/ChOx&HRP in phosphatic buffer solution (0.02 M, pH 7.5) at 37 °C. (C) The linear standard curve for cholesterol determination. Inset: the corresponding images of the colored products. (D) Absorbance of the solutions with different interfering substances or cholesterol for demonstrating selectivity of cholesterol detection. The concentration was 10 mM for cholesterol, and 50 mM for the other interfering substances.

Table 1
Determination of cholesterol in serum samples (n = 3).

Samples	Spiked (mM)	Found (mM)	Recovery (%)	RSD (%)
Serum 1	0.00	2.01	–	3.7%
	1.00	2.94	93.0%	5.8%
	1.50	3.43	94.7%	3.3%
	2.00	4.13	106.0%	4.0%
Serum 2	0.00	1.73	–	6.2%
	1.00	2.67	94.0%	2.1%
	1.50	3.36	108.7%	1.5%
	2.00	3.71	99.0%	2.3%
Serum 3	0.00	1.88	–	2.7%
	1.00	2.79	91.0%	1.7%
	1.50	3.38	100.0%	3.4%
	2.00	3.97	104.5%	2.3%

Cholesterol solutions with different concentrations were reacted with PCN-333/ChOx&HRP suspension at 37 °C for 30 min to assess the linear range and detection limit and determine cholesterol under the optimized conditions. The acetate buffer solution and ABTS were added to react for 10 min. As the cholesterol content in the solution increased, its color deepened (Fig. 3B and C). A good linearity between the absorbance at 418 nm and the concentration of cholesterol in the range of 0.0–40.0 μM was observed. The linear fitting equation was $A_{418\,nm} = 0.02089 + 0.0343 \times$. The limit of detection (LOD) was calculated based on the standard deviation (SD) of the responses of the blank sample and the slope (S) of the calibration curve (Fig. 3C). The LOD value for cholesterol detection is 0.6 μM according to the formula of LOD = 3 SD/S. The LOD was much improved compared with that of recently reported colorimetric detections of cholesterol [40,44]. The cutoff value of cholesterol in the blood of patients with hypercholesterolemia is about 6 mM [45]. Therefore, the PCN-333/ChOx&HRP-based detection system was sufficiently sensitive to distinguish normal individuals from patients with diseases.

The selective test for the evaluation of the performance of a sensor is an important factor. Cholesterol and other various kinds of interference in serum compounds should be tested to verify the selectivity of PCN-333/ChOx&HRP. Potential interferences, such as glucose, ascorbic acid, cysteine, histidine, arginine, lysine, glycine, and ATP, were added to the reaction system, and the results showed that they exhibited low absorbance at 418 nm, and only cholesterol showed significant absorbance (Fig. 3D), although the concentration of glucose and ascorbic acid were 15 times higher than that of cholesterol and the concentration of the rest of interfering substances **w**ere 7.5 times higher than that of cholesterol. Therefore, the results indicated that PCN-333/ChOx&HRP had a high selectivity for cholesterol detection.

3.4. Detection of cholesterol in serum

To verify whether our method could be used for practical applications, we used it to detect actual samples. The standard addition method was utilized to analyze the serum samples. The serum was diluted with the standard solutions of different concentrations. The cholesterol levels of the three volunteers were 2.01, 1.73, and 1.88 mM (Table 1). These detected values well agreed with the values of 2.07, 1.77, and 1.84 mM, which were determined by using a conventional free ChOx-HRP method (Table S1). The recovery of the detected cholesterol of the serum was 91.0–108.7%, and the different concentrations of the cholesterol levels of RSD were less than 6.2%, confirming that this method had good accuracy and reliability (Table 1 and Table S1).

4. Conclusions

A simple and highly efficient strategy was demonstrated for the surface adsorption and pore encapsulation of bi-enzymes by considering the high surface area and high concentration of mesoporous cages of MOFs (i.e., PCN-333). The co-immobilized ChOx and HRP showed a high catalytic activity in a cascade reaction. With the rigid MOF structures, the co-immobilized enzymes not only had high tolerance to protease digestion, organic solvents, and pH and thermal variation but also had a long shelf life. A convenient colorimetric method was established to sensitively and selectively detect cholesterol. These findings indicated that MOFs that absorbed and encapsulated multi-enzymes might be used in detection of cholesterol in serum samples.

Acknowledgment

This work was supported the National Natural Science Foundation of China (21275097), the Natural Science Foundation of Shaanxi Province (2018JM2005), the Fundamental Research Funds for the Central Universities (GK201602010), and the 111 Project (B14041).

Interests statement

There are no competing interests to declare.

Appendix A. Supplementary material

Supplementary data associated with this article can be found in the online version at doi:10.1016/j.talanta.2019.03.060.

References

[1] M.C. van Oers, F.P. Rutjes, J.C. van Hest, Cascade reactions in nanoreactors, Curr. Opin. Biotechnol. 28 (8) (2014) 10–16.
[2] M. Marguet, C. Bonduelle, S. Lecommandoux, ChemInform abstract: multi-compartmentalized polymeric systems: towards biomimetic cellular structure and function, Chem. Soc. Rev. 42 (2) (2013) 512–529.
[3] J. Cui, S. Ren, B. Sun, S. Jia, Optimization protocols and improved strategies for metal-organic frameworks for immobilizing enzymes: current development and future challenges, Coord. Chem. Rev. 370 (2018) 22–41.
[4] M.L. Verma, M. Puri, C.J. Barrow, Recent trends in nanomaterials immobilised enzymes for biofuel production, Crit. Rev. Biotechnol. 36 (1) (2016) 108–119.
[5] D.C. Jian, R.J. Shi, Optimization protocols and improved strategies of cross-linked enzyme aggregates technology: current development and future challenges, Crit. Rev. Biotechnol. 35 (1) (2015) 15–28.
[6] R.A. Sheldon, S.V. Pelt, Enzyme immobilisation in biocatalysis: why, what and how, Chem. Soc. Rev. 42 (15) (2013) 6223–6235.
[7] D.J. Tranchemontagne, J.L. Mendoza-Cortes, M. O'Keeffe, O.M. Yaghi, ChemInform abstract: secondary building units, nets and bonding in the chemistry of metal-organic frameworks, Chem. Soc. Rev. 40 (29) (2009) 1257–1283.
[8] W. Wei, S. Dong, G. Huang, Q. Xie, T. Huang, MOF-derived Fe_2O_3 nanoparticle embedded in porous carbon as electrode materials for two enzyme-based biosensors, Sens. Actuators B. 260 (2018) 189–197.
[9] Q. Zhu, W. Zhuang, Y. Chen, Z. Wang, B.V. Hernandez, J. Wu, P. Yang, D. Liu, C. Zhu, H. Ying, Nano-Biocatalysts of Cyt c@ZIF-8/GO Composites with High Recyclability via a de Novo Approach, ACS Appl. Mater. Interfaces 10 (2018) 16066–16076.
[10] X. Lian, Y. Fang, E. Joseph, Q. Wang, J. Li, S. Banerjee, C. Lollar, X. Wang, H.C. Zhou, Enzyme-MOF (metal-organic framework) composites, Chem. Soc. Rev. 46 (11) (2017) 3386–3401.
[11] P. Li, S.Y. Moon, M.A. Guelta, S.P. Harvey, J.T. Hupp, O.K. Farha, Encapsulation of a nerve agent detoxifying enzyme by a mesoporous zirconium metal-organic framework engenders thermal and long-term stability, J. Am. Chem. Soc. 138 (26) (2016) 8052–8055.
[12] G.Y. Jeong, R. Ricco, K. Liang, J. Ludwig, J.O. Kim, P. Falcaro, D.P. Kim, Bioactive MIL-88A framework hollow spheres via interfacial reaction in-droplet microfluidics for enzyme and nanoparticle encapsulation, Chem. Mater. 27 (23) (2015) 479–494.
[13] L. Wang, Y. Song, Y. Shen, C. Gong, J. Chen, M. Xu, L. Wang, A. Novel Glucose, Biosensor based on Tb@ mesoporous metal-organic frameworks/carbon nanotube nanocomposites, ChemElectroChem 4 (2017) 1457–1462.
[14] Y. Li, J. Liu, K. Zhang, L. Lei, Z. Lei, UiO-66-NH_2@PMAA: a hybrid polymer -MOFs architecture for pectinase immobilization, Ind. Eng. Chem. Res. 57 (2) (2018) 559–567.
[15] S. Jung, S. Park, Dual-surface functionalization of metal organic frameworks for enhancing the catalytic activity of candida antarctica lipase B in polar organic media, ACS Catal. 7 (1) (2017) 438–442.
[16] Y.H. Shih, S.H. Lo, N.S. Yang, B. Singco, Y.J. Cheng, C.Y. Wu, I.H. Chang, H.Y. Huang, C.H. Lin, Trypsin-immobilized metal–organic framework as a biocatalyst in proteomics analysis, ChemPlusChem 77 (11) (2012) 982–986.
[17] X. Wu, M. Hou, J. Ge, Metal-organic frameworks and inorganic nanoflowers: a type of emerging inorganic crystal nanocarrier for enzyme immobilization, Catal. Sci. Technol. 5 (12) (2015) 5077–5085.

[18] E. Gkaniatsou, C. Sicard, R. Ricoux, J.P. Mahy, N. Steunou, C. Serre, Metal-organic frameworks: a novel host platform for enzymatic catalysis and detection, Mater. Horiz. 4 (1) (2016) 55–63.
[19] M.B. Majewski, A.J. Howarth, P. Li, M.R. Wasielewski, J.T. Hupp, O.K. Farha, Enzyme encapsulation in metal-organic frameworks for applications in catalysis, CrystEngComm 19 (29) (2017) 4082–4091.
[20] H.S. Wang, Metal–organic frameworks for biosensing and bioimaging applications, Coord. Chem. Rev. 349 (2017) 139–155.
[21] K. Liang, C.J. Coghlan, S.G. Bell, C. Doonan, P. Falcaro, Enzyme encapsulation in zeolitic imidazolate frameworks: a comparison between controlled co-precipitation and biomimetic mineralisation, Chem. Commun. 52 (3) (2015) 473–476.
[22] T.J. Pisklak, M. Macías, D.H. Coutinho, R.S. Huang, K.J.B. Jr, Hybrid materials for immobilization of MP-11 catalyst, Top. Catal. 38 (4) (2006) 269–278.
[23] D. Feng, T.F. Liu, J. Su, M. Bosch, Z. Wei, W. Wan, D. Yuan, Y.P. Chen, X. Wang, K. Wang, Stable metal-organic frameworks containing single-molecule traps for enzyme encapsulation, Nat. Commun. 6 (3) (2015) 5979.
[24] H.S. Lan, R. Duncan, A.H. Schob, S.C. Chakko, R. Mulingtapang, J.L. He, G.O. Perez, Serum levels of high-density lipoprotein phospholipids correlate inversely with severity of angiographically defined coronary artery disease, Atherosclerosis 152 (2) (2000) 469–473.
[25] K. Wang, H. Ren, N. Li, X. Tan, F. Dang, Ratiometric fluorescence sensor based on cholesterol oxidase-functionalized mesoporous silica nanoparticle@ZIF-8 core-shell nanocomposites for detection of cholesterol, Talanta 188 (2018) 708–713.
[26] Y.T. Lin, S.S. Wu, H.L. Wu, Highly sensitive analysis of cholesterol and sitosterol in foods and human biosamples by liquid chromatography with fluorescence detection, J. Chromatogr. A 1156 (1) (2007) 280–287.
[27] L. Yang, H. Zhao, Y. Li, X. Ran, G. Deng, Y. Zhang, H. Ye, G. Zhao, C.P. Li, Indicator displacement assay for cholesterol electrochemical sensing using a calix[6]arene functionalized graphene-modified electrode, Analyst 141 (1) (2015) 270–278.
[28] U. Saxena, M. Chakraborty, P. Goswami, Covalent immobilization of cholesterol oxidase on self-assembled gold nanoparticles for highly sensitive amperometric detection of cholesterol in real samples, Biosens. Bioelectron. 26 (6) (2011) 3037–3043.
[29] S. Nantaphol, O. Chailapakul, W. Siangproh, Sensitive and selective electrochemical sensor using silver nanoparticles modified glassy carbon electrode for determination of cholesterol in bovine serum, Sens. Actuators B 207 (207) (2015) 193–198.
[30] Y. Li, H. Bai, Q. Liu, J. Bao, M. Han, Z. Dai, A nonenzymatic cholesterol sensor constructed by using porous tubular silver nanoparticles, Biosens. Bioelectron. 25 (10) (2010) 2356–2360.
[31] C. Zhao, L. Wan, L. Jiang, Q. Wang, K. Jiao, Highly sensitive and selective cholesterol biosensor based on direct electron transfer of hemoglobin, Anal. Biochem. 383 (1) (2008) 25.
[32] X. Cai, X. Gao, L. Wang, Q. Wu, X. Lin, A layer-by-layer assembled and carbon nanotubes/gold nanoparticles-based bienzyme biosensor for cholesterol detection, Sens. Actuators, B 181 (5) (2013) 575–583.
[33] A. Umar, R. Ahmad, S.W. Hwang, S.H. Kim, A. Al-Hajry, Y.B. Hahn, Development of highly sensitive and selective cholesterol biosensor based on cholesterol oxidase co-immobilized with α-Fe_2O_3 micro-pine shaped hierarchical structures, Electrochim. Acta 135 (2014) 396–403.
[34] A. Aghaei, M.R.M. Hosseini, M. Najafi, A novel capacitive biosensor for cholesterol assay that uses an electropolymerized molecularly imprinted polymer, Electrochim. Acta 55 (5) (2010) 1503–1508.
[35] C.H. Grün, S. Besseau, Normal-phase liquid chromatography-atmospheric-pressure photoionization-mass spectrometry analysis of cholesterol and phytosterol oxidation products, J. Chromatogr. A 1439 (2015) 74–81.
[36] B. Cañabate-Díaz, A.S. Carretero, A. Fernández-Gutiérrez, A.B. Vega, A.G. Frenich, J.L.M. Vidal, J.D. Martos, Separation and determination of sterols in olive oil by HPLC-MS, Food Chem. 102 (3) (2007) 593–598.
[37] N.R. Nirala, S. Pandey, A. Bansal, V.K. Singh, B. Mukherjee, P.S. Saxena, A. Srivastava, Different shades of cholesterol: gold nanoparticles supported on MoS_2 nanoribbons for enhanced colorimetric sensing of free cholesterol, Biosens. Bioelectron. 74 (2015) 207–213.
[38] J. Castroperez, S.F. Previs, D.G. Mclaren, V. Shah, K. Herath, G. Bhat, D.G. Johns, S.P. Wang, L. Mitnaul, K. Jensen, In vivo D_2O labeling to quantify static and dynamic changes in cholesterol and cholesterol esters by high resolution LC/MS, J. Lipid Res. 52 (1) (2011) 159–169.
[39] N.R. Nirala, S. Abraham, V. Kumar, A. Bansal, A. Srivastava, P.S. Saxena, Colorimetric detection of cholesterol based on highly efficient peroxidase mimetic activity of graphene quantum dots, Sens. Actuators B 218 (2015) 42–50.
[40] M. Chung, Y.J. Jang, M.I. Kim, Convenient colorimetric detection of cholesterol using multi-enzyme co-incorporated organic-inorganic hybrid nanoflowers, J. Nanosci. Nanotechnol. 18 (9) (2018) 6555–6561.
[41] L. Xu, Z. Zhang, X. Fang, Y. Liu, B. Liu, J. Liu, Robust hydrogels from lanthanide nucleotide coordination with evolving nanostructures for a highly stable protein encapsulation, ACS Appl. Mater. Interface 10 (2018) 14321–14330.
[42] U. Saxena, A.B. Das, Nanomaterials towards fabrication of cholesterol biosensors: key roles and design approaches, Biosens. Bioelectron. 75 (2016) 196–205.
[43] X. Lian, Y. Huang, Y. Zhu, Y. Fang, R. Zhao, E. Joseph, J. Li, J.P. Pellois, H.C. Zhou, Enzyme-MOF nanoreactor activates nontoxic paracetamol for cancer therapy, Angew. Chem. Int. Ed. 57 (2018) 5725–5730.
[44] M.I. Kim, J. Shim, T. Li, J. Lee, H.G. Park, Fabrication of nanoporous nanocomposites entrapping Fe_3O_4 magnetic nanoparticles and oxidases for colorimetric biosensing, Chem. Eur. J. 17 (38) (2011) 10700–10707.
[45] D.R. Nair, M. Sharifi, K. Al-Rasadi, Familial hypercholesterolaemia, Curr. Opin. Cardiol. 29 (4) (2014) 381–388.